Journal of Materials Science: Materials in Electronics (2020) 31:4473–4478
https://doi.org/10.1007/s10854-020-02984-w

Thermal annealing of AlN films for piezoelectric applications

Etienne Herth[1] · Dame Fall[2] · Jean-Yves Rauch[2] · Virginie Mourtalier[2] · Grégory Guisbiers[3]

Received: 4 December 2019 / Accepted: 23 January 2020 / Published online: 14 February 2020
© Springer Science+Business Media, LLC, part of Springer Nature 2020

Abstract
Aluminum nitride is an excellent electrical insulator and important piezoelectric material making it suitable for a wide range of applications in electronics and optoelectronics. However, to exhibit and preserve those piezoelectric properties, care has to be taken during manufacturing process. Indeed, the *c*-axis crystalline orientation of AlN is a necessary condition for piezoelectricity. Therefore, the goal of this paper is to compare AlN films grown on (100) silicon substrate by pulsed reactive DC sputtering at 400 °C on top of three different metallic underlayer electrodes (Ti/Pt, Cr/Pt, and AlN/Cr/Pt) by preserving the crystalline properties not only at room temperature but also at high temperatures. Among all deposited AlN films on top of the metallic underlayer electrode, only AlN/Cr/Pt has kept its crystallinity up to 950 °C.

1 Introduction

Obtaining high-quality Aluminum nitride (AlN) films on different metallic underlayer electrodes has already been demonstrated in several applications [1–8]. Indeed, there is an increasing demand for high-temperature electronic components for sensors in aerospace and aircraft applications. AlN is a promising piezoelectric material able to maintain its piezoelectricity up to 1200 °C [9]. The selection of materials in MEMS is an important topic [10–14]. The systematic approach to select the manufacturing process [15] and materials applied to MEMS has already began [16, 17]. The selection of underlayer electrode is essential to achieve high-quality piezoelectric AlN films. The influence of the deposition parameters (i.e., temperature, power, and gas flows) and the type of metallic underlayer electrodes on the film texture were investigated by using the full width at half maximum (FWHM) of the (002) rocking curve measurement. Several bottom layers, such as Ti/Mo [18], Ti/TiN [19], Cr/Pt [20], Al [21], Ti/Pt [22], and AlN/Pt [23], were deposited by a sputtering process in order to find out the best lattice mismatch between the piezoelectric AlN lattice parameter and the lattice parameter of the as-deposited bottom layer. The piezoelectric properties of AlN films are obtained from columnar grains with (0 0 2) crystal orientation, while the crystal planes of the underlayer electrodes are Al (1 1 1), Pt (1 1 1), Ti (0 0 2) and Mo (1 1 0), TiN (1 1 1), Cr (110). Up to now, the best crystalline structure was obtained by sputtering AlN films on platinum (Pt) substrates [24]. Furthermore, heating AlN at a very high furnace temperature (1100 °C) shows an improvement in its *c*-axis crystal orientation [25].

In this study, the structural properties of the AlN and bottom electrode (Ti/Pt, Cr/Pt, and AlN/Cr/Pt) films and the effect of rapid thermal annealing were investigated by XRD and AFM techniques for sustainability and reliability in low- and high-temperature applications. Although the underlayer electrodes of piezoelectric films are well tabulated (e.g., stress, resistivity, thermal expansion coefficients, and strength), few data are available on the grain rearrangements caused by high-temperature annealing [26–28] as well as the risk of diffusion [29, 30]. Our motivation was to demonstrate that we can efficiently harvest the individual advantages and limitations of the metallic underlayer electrodes and AlN film. This work focused on the development of high-quality AlN thin films with *c*-axis orientation. This reproducibility requires a deep understanding of the crystallization mechanisms and the critical processing parameters controlling the pre-deposition conditions (viz. the precursors and the

✉ Etienne Herth
etienne.herth@c2n.upsaclay.fr

[1] Centre de Nanosciences et de Nanotechnologies, CNRS UMR 9001, Univ. Paris-Sud, Université Paris-Saclay, 91120 Palaiseau, France

[2] FEMTO-ST, Université de Franche Comté, UBFC, CNRS UMR 6174-25044, Besançon, France

[3] Department of Physics & Astronomy, University of Arkansas at Little Rock, 2801 South University Avenue, Little Rock, AR 72204, USA

choice of the electrode) and the post-deposition (viz. annealing treatment) conditions. Experiments were performed in order to understand the mechanisms by which such textures were obtained on identical silicon substrates by using the same depositions conditions.

2 Experimental

Piezoelectric AlN films have been deposited in a pulsed reactive DC sputtering of pure Aluminum target (Al 99.99 % pure) in an Ar/N_2 gas mixture, on bottom metal electrodes previously covered on the Si (100) substrate. Because Pt thin films show poor adhesion to semiconductor and dielectric substrates [31, 32], titanium (Ti) and chromium (Cr) were chosen as an adhesion layer. Platinum (Pt) was chosen as a metallic component of bottom electrodes due to its crystal planes orientation, which present a hexagonal orientation (002) for the growth of wurtzite AlN. As samples tests, we used chips (1×1 cm^2) of silicon-based (100) Si wafers. The latter were first heated at 200 °C for 15 min in order to degas the surface of all adsorbed species and stay at this temperature for the entire cycle of sputtering process. The silicon wafer was then etched at 150 W RF for 5 min in a pure Argon (Ar) flow of 10 sccm at a pressure of 7×10^{-3} mbar. Two Ti/Pt electrodes (10/ 300 nm thick) and Cr/Pt (10/300 nm thick) were sputtered in a PVD Plassys machine on wafer heated at 300 °C, using a pressure of 7×10^{-3} mbar and a flow Argon of 10 sccm. The Ti/Pt and Cr/Pt were sputtered without bias power, respectively, at 1 A (adhesion layer) and 0.6 A (bottom metal). The AlN was deposited at 400 °C in another PVD machine (Sigma Fxp trikon) with an input power of 5.75 kW, Ar/N_2 ratio of 125/500 sccm and a pressure of 4×10^{-3} mbar.

The films have been characterized by X-ray diffraction (XRD) and tapping mode atomic force microscopy (AFM) as shown in Figs. 1 and 2.

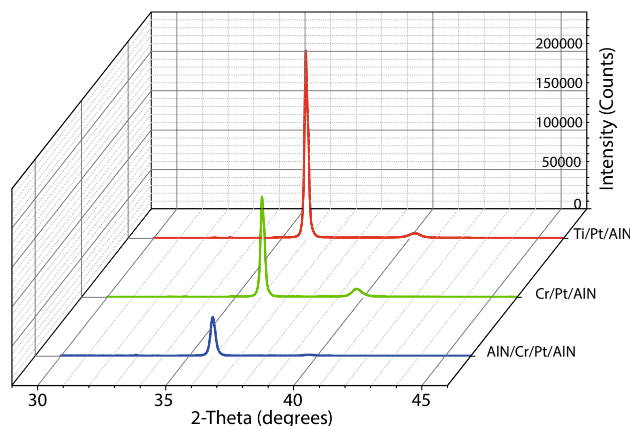

Fig. 2 Typical X-ray diagrams of a 1-μm-thick piezoelectric AlN film deposited onto different electrodes: Ti/Pt, Cr/Pt, and AlN/Cr/Pt

3 Results

First, the surface morphology (i.e., film surface roughening and grain coarsening processes) of the film's layers was analyzed by Atomic Force Microscopy (AFM) with a Nanoscope IIIa equipment (from Digital Instruments, CA) operating in tapping mode under ambient conditions. In Fig. 1, three AlN film surface morphologies were measured by AFM as a function of underlayer electrode. These investigations revealed that the grain size was increased for AlN/Cr/Pt. Table 1 shows that the average of the root mean square (rms) surface roughness R_{rms} is within a range from 2.34 up to 5.35 nm depending on the electrode. For Cr/Pt and AlN/Cr/Pt, the R_{rms} is shown to gradually increase with the AlN thickness.

Then, the morphology of the AlN film can be characterized by its fractal dimension $D_{fractal}$ using the WSxM software [33]. Considering the morphology of the film as a surface containing lakes within islands and islands within lakes, the fractal dimension measured is [34–36]:

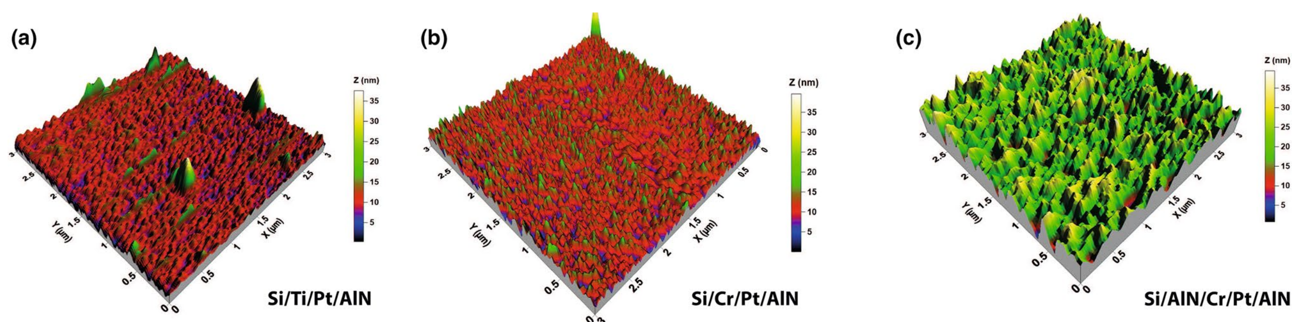

Fig. 1 AFM pictures of surface morphologies (3×3 μm^2) of the AlN deposited by a pulsed reactive DC sputtering on different electrodes: **a** Ti/Pt, **b** Cr/Pt, and **c** AlN/Cr/Pt

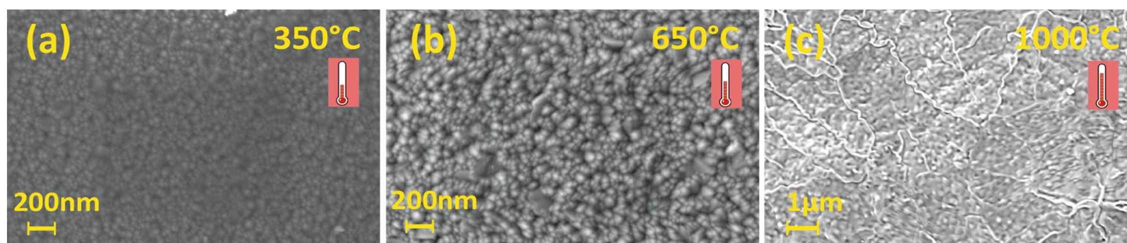

Fig. 3 SEM micrographs of AlN/Cr/Pt/AlN thin films at various temperatures from 350 to 1000 °C

$$D'_{\text{fractal}} = D_{\text{fractal}} - 1 \tag{1}$$

The surface of the island A is linked to its radius R by the relationship $A \infty R^2$. And the perimeter of the island P is linked to the fractal dimension of the thin film D'_{fractal} with the relation $P \infty R^{D'_{\text{fractal}}}$ and is given by

$$P = \mu A^{\alpha_{\text{fractal}}} \tag{2}$$

where μ is the proportionality factor between the perimeter and the surface, $\alpha_{\text{fractal}} = D'_{\text{fractal}}/2$. As shown in Table 1, the fractal dimension of Ti/Pt/AlN films is turned to 1.26 and close to 1.13 of Cr/Pt/AlN , while AlN/Cr/Pt/AlN is around 1.45. It has been shown that the fractal dimension is related to the film growth mode [34]. A fractal dimension D'_{fractal} around 1.5 is a characteristic of a Volmer–Weber growth mode. This confirms the columnar growth of AlN/Cr/Pt/AlN.

After deposition of AlN and underlayer electrodes, the crystalline structure was analyzed by XRD $\theta - 2\theta$ pattern in the range of 30° to 50°. Fig. 1 shows the XRD patterns obtained by Ti/Pt/AlN, Cr/Pt/AlN, and AlN/Cr/Pt/AlN as deposited on silicon wafer. The crystallites of the piezoelectric AlN film are perfectly (0002) oriented onto the electrodes. X-ray measurements presented in Fig. 2 show that the adhesion layers Ti and Cr had no significant influence on the AlN c-axis orientation. Excellent crystallinity was obtained on the Ti/Pt and Cr/Pt metal electrodes, while a poor crystallinity of AlN deposited on the underlayer electrode AlN/Cr/Pt was observed.

In addition, the multilayer AlN electrode employed in sensors applications should offer a thermal stability and a good piezoelectricity response. Among them, surface acoustic wave (SAW) sensors are a promising solution to read temperature wirelessly in harsh environments up to 900 °C for a few tens of hours has been demonstrated [37, 38]. Most of these devices are based on Langasite (LGS), Langatate (LGT) bulk materials which do not lose their piezoelectric properties at high temperatures. However, some efforts have been dedicated to explore the AlN film performances at high temperatures [39, 40]. Indeed, the annealing process strongly depends on the process

Table 1 AlN roughness and fractal dimension values were obtained on different electrodes at ambient temperature

Materials	Thickness (nm)	D'_{fractal}	R_{rms} (nm)
Ti/Pt/AlN	10/600/1000	1.26	2.52
Cr/Pt/AlN	10/600/1000	1.13	2.34
AlN/Cr/Pt /AlN	1000 /10/600/1000	1.45	5.35

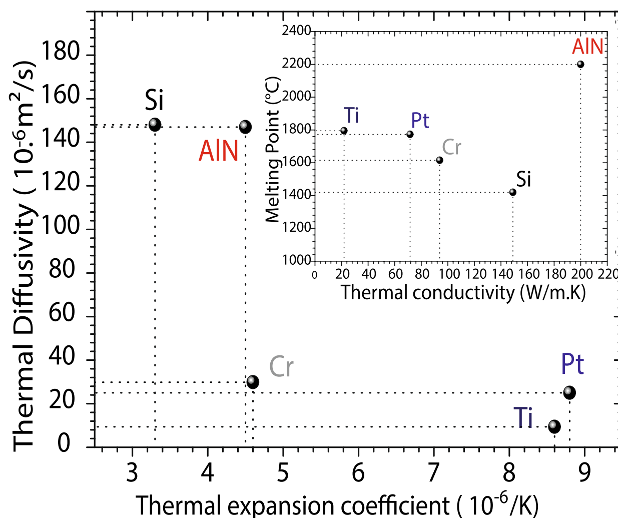

Fig. 4 Material properties of the AlN and metallic underlayer electrodes

parameters, which include temperature, ambient atmosphere, annealing ramp, and annealing time. At high temperatures, this multilayer can be damaged due to the difference in the thermal expansion coefficient and/or diffusivity between Si, AlN, and the metal underlayer electrodes (see Fig. 3). Material properties such as thermal conductivity, melting point, and thermal expansion coefficient of the AlN and metal underlayers are presented in Fig. 4. AlN is considerably better than others (Si, Pt, Ti, Cr) in terms of thermal conductivity and melting point. Beyond this temperature, diffusion, and cracks appear. Thermal diffusivity $= k/\rho C$, where k = thermal conductivity, ρ = density and C = heat capacity. One solution is to use the AlN/ metallic

underlayers electrodes/AlN like a protective overlayer up to 600 °C.

Much attention has been focused on the RTA process. After deposition of the AlN piezoelectric thin films on each underlayer electrode, the stacks were annealed in N_2 atmosphere at temperatures from 350 °C, 450 °C, 650 °C, 950 °C, and 1000 °C during 30 min, 10 min, 5 min, 2 min, and 1 min, respectively, and the ramp fixed at 10 °C/min. Each sample was cut into several pieces (1cm x 1cm) that were subjected to different RTA processes. The multilayer AlN metal electrode may be degraded by a high thermal treatment. As shown in Fig. 3, for annealing temperatures from 350 to 650 °C the grain sizes become larger while for annealing temperatures of 1000 °C, cracks appeared in the films. However, the crystallinity seems to be improved by rapid thermal optimized annealing. X-ray investigation revealed that the film's crystallinity was improved by rapid thermal annealing. Indeed as shown in Fig. 5, AlN films were purely oriented with the *c*-axis perpendicular to the growth plane (i.e., AlN peak at 36°). For example, the crystallinity of AlN/Cr/Pt/AlN increases as the annealing temperature increases, we can note that FWHM decreases while the intensity of X-Ray increases at high temperatures. Thus, after annealing at 350 °C, the peak becomes more intense and narrower, which indicates an increase in the grain size of the original crystallites. According to Fig. 4, the thermal diffusivity for Si substrate and the AlN films are quite similar (close to 1.5×10^{-4} m^2 s^{-1}) and better than the other underlayer electrodes. The disadvantage of the metallic electrodes is mainly due to their high diffusivity. Consequently, metallic atoms migrate at high temperatures predominantly along grain boundaries through the AlN film. This diffusion leads to a decrease the AlN film crystallinity, especially at high temperatures. An important aspect of this work was to provide thermal stability that would make it an attractive AlN-stacked film material application in harsh environments.

Moreover, all the deposited films have kept their crystallinity up to 950 °C with an annealing time of from 1 min to 30 min. However, at 950 °C and 1100 °C annealing temperature, the deposited AlN film on the metallic underlayer electrodes Ti/Pt and Cr/Pt was no longer crystalline. Only, the AlN film deposited, respectively, on the underlayer electrode AlN/Cr/Pt maintained its crystalline properties up to 950 °C as presented in Fig. 6.

4 Discussion

Depositing AlN films at room temperature is a "must," since a high-temperature process during film growth is not necessarily compatible with all the manufacturing steps of device fabrication. Thus, reactive sputtering operating at low processing temperature is the best process to control film properties. As far as the substrate temperature is concerned, Medjani et al. [42] showed that lower (below 400 °C) temperature was favorable to the formation of (002) plane, while Jin et al. [1] concluded that the 430 °C was the optimal temperature to maximize the *c*-axis preferred orientation.

In this work, XRD measurements on AlN films show that an annealing treatment with the temperature range from 350 to 400 °C improves the crystalline quality (see Table 2). Without an annealing treatment (viz. ambient temperature 25 °C, and/or as-deposited films), the higher quality of the AlN films observed was obtained mostly on the bottom electrode. Herein, the crystallinity of the electrodes Cr/Pt and Ti/Pt is mainly influenced by the sputtering parameters and not by the substrate(Silicon or AlN interlayer). This means that the AlN interlayer has a

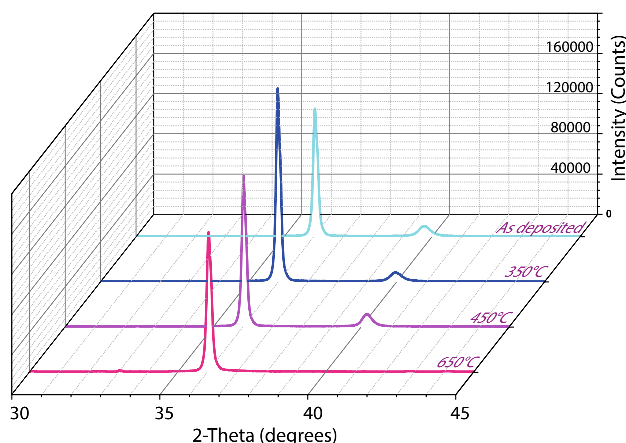

Fig. 5 X-ray diagrams of a 1-μm-thick piezoelectric AlN/Cr/Pt/AlN coating on silicon as a function of annealing temperatures. Annealing time was fixed to 10 min for all samples

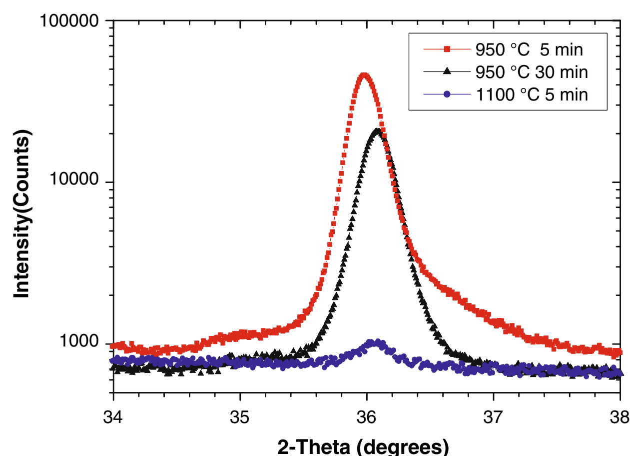

Fig. 6 X-ray diagrams of a 1-μm-thick piezoelectric AlN/Cr/Pt/AlN coating on silicon substrate as a function of annealing temperatures

Table 2 Comparison between our work and previous research concerning the temperature resistance of AlN films by using an annealing treatment in N_2 atmosphere of each sample

Annealing treatment	Sample	Thermal stability	Optimized FWHM
Our work	Si/Ti/Pt/AlN	950 °C ⟶ 30 min	0.170° @ 25 °C/as-deposited 0.160° @ 350 °C/30 min
	Si/Cr/Pt/AlN	950 °C ⟶ 30 min	$0.186° @ 25 °C/as-deposited 0.164° @ 350 °C/30 min
	Si/AlN/Cr/Pt/AlN	1100 °C ⟶ 5 min	0.221° @ 25 °C/as-deposited 0.170° @ 350 °C/5 min
Reference [25]	Si/Mo/AlN/Mo	1100 °C ⟶ N.C.	0.184° @ 25 °C/as-deposited 0.1673° @ 1100 °C
Reference [39]	Si/SiO_2/AlN	1300 °C ⟶ 30 s	N.C.
Reference [41]	Sapphire/AlN	1000 °C ⟶ 10 s	N.C.

minor role on the crystallization of Ti/Pt and Cr/Pt electrodes. Furthermore, as shown in Table 2, thermal annealing improved the AlN crystalline quality, as confirmed by the lower FWHM value. The FWHM of an AlN deposited on the Cr/Pt electrode was improved from 1.7° to 1.6°. The deposition conditions (viz. the choice of the metal electrode) and the post-deposition annealing treatment give some insight into the orientation of the AlN films and their reliability.

Compared with other common annealing treatment [25, 39, 41], our data suggest that Cr/Pt/AlN would display a good FWHM at lower temperature treatment, while AlN/Cr/Pt/AlN can be stable until 1000 °C during 5 min. Although we show the advantages of the annealing treatment, it is difficult to prepare stable and high-quality crystal-oriented AlN films on bottom electrodes at high temperature for long period of time. Moreover, we also grew AlN films on Cr/Pt/AlN electrodes by inserting AlN interlayer between the bottom electrodes and silicon substrate, such as AlN/ Cr/Pt/AlN/Si. We observed that at high temperatures, the stability and orientation of the AlN film and Cr/Pt electrode were preserved by the AlN interlayer, because this interlayer is very effective by decreasing the diffusion of the Cr/Pt electrode.

The study of the thermal stability of the metallization electrodes summarized in Table 2 revealed that no microcracks were observed. Ayazi et al. show that an improvement in FWHM translates into better transduction efficiency from the AlN layer and should result in lower insertion loss and a higher quality factor for sensors [25]. The successful preparation of well-oriented crystalline AlN films with optimized FWHM suggests AlN film having a low-loss, good high-frequency characteristics together with a high piezoelectric coupling coefficient. By the comprehensive characterization of the AlN/Cr/Pt/AlN films, it is shown that the process conditions did not degrade the above-discussed device-relevant material properties. In order to see the potential of the bimorph piezoelectric system, for piezoelectric energy harvesting, we demonstrate herein that AlN/Cr/Pt/AlN will be a promising candidate [43].

5 Conclusion

In summary, highly *c*-axis-oriented AlN thin films have been investigated as function of the different metallic underlayer electrodes deposited by the well-established PVD technique with annealing post-treatment. Meanwhile, the reduction in (002) diffraction peak reveals that higher annealing temperature can deteriorate the crystalline quality, which is due to enhanced diffusion. The choice of temperature and annealing time must, therefore, be carefully chosen in order to avoid damaging the AlN film and consequently enhance its crystal quality. In conclusion, the FWHM width of 1-µm-thick AlN deposited on Ti/Pt shows a better crystal quality with low roughness, while the use of AlN/Cr/Pt/AlN is one possible solution to strongly hinder the cracks up to 950 °C.

Acknowledgements This work was partly supported by the French RENATECH network with FEMTO-ST and C2N as technological facilities.

References

1. H. Jin, B. Feng, S. Dong, C. Zhou, J. Zhou, Y. Yang, T. Ren, J. Luo, D. Wang, J. Electron. Mater. **41**(7), 1948 (2012)
2. T. Hu, S. Mao, C. Chao, M. Wu, H. Huang, D. Gan, J. Electron. Mater. **36**(1), 81 (2007)
3. E. Herth, L. Valbin, F. Lardet-Vieudrin, E. Algré, Microsyst. Technol. **23**(9), 3873 (2017). https://doi.org/10.1007/s00542-015-2727-9
4. O. Mareschal, S. Loiseau, A. Fougerat, L. Valbin, G. Lissorgues, S. Saez, C. Dolabdjian, R. Bouregba, G. Poullain, IEEE Trans. Ultrason. Ferroelectr. Freq. Control **57**(3), 513 (2010). https://doi.org/10.1109/TUFFC.2010.1441
5. E. Herth, E. Algré, J.Y. Rauch, J.C. Gerbedoen, N. Defrance, P. Delobelle, Phys. Stat. Solidi A **213**(1), 114 (2016). https://doi.org/10.1002/pssa.201532302
6. A. Pandey, S. Dutta, R. Prakash, R. Raman, A.K. Kapoor, D. Kaur, J. Electron. Mater. **47**(2), 1405 (2018)
7. K. Jones, M. Derenge, T. Zheleva, K. Kirchner, M. Ervin, M. Wood, R. Vispute, R. Sharma, T. Venkatesan, J. Electron. Mater. **29**(3), 262 (2000)

8. K. Jones, M. Derenge, P. Shah, T. Zheleva, M. Ervin, K. Kirchner, M. Wood, C. Thomas, M. Spencer, O. Holland et al., J. Electron. Mater. **31**(6), 568 (2002)
9. R.C. Turner, P.A. Fuierer, R.E. Newnham, T.R. Shrout, Appl. Acoust. **41**(4), 299 (1994). https://doi.org/10.1016/0003-682X(94)90091-4
10. R. Roth, F. Field, J. Clark, J. Comput. Aided Mater. Des. **1**(3), 325 (1994). https://doi.org/10.1007/BF00712855
11. M.F. Ashby, D. Cebon, J. Phys. IV **03**(C7), C7 (1993). https://doi.org/10.1051/jp4:1993701
12. M.F. Ashby, Acta Mater. **48**(1), 359 (2000). https://doi.org/10.1016/S1359-6454(99)00304-3
13. J. Qian, Y.P. Zhao, Mater. Des. **23**(7), 619 (2002). https://doi.org/10.1016/S0261-3069(02)00051-1
14. M.F. Ashby, Y.J.M. Bréchet, D. Cebon, L. Salvo, Mater. Des. **25**(1), 51 (2004). https://doi.org/10.1016/S0261-3069(03)00159-6
15. D. Quinn, S. Spearing, M. Ashby, N.A. Fleck, J. Microelectromech. Syst. **15**(5), 1039 (2006). https://doi.org/10.1109/JMEMS.2006.880292
16. R.V. Rao, Mater. Sci. Eng. A **431**(1–2), 248 (2006). https://doi.org/10.1016/j.msea.2006.06.006
17. G. Guisbiers, E. Herth, B. Legrand, N. Rolland, T. Lasri, L. Buchaillot, Microelectron. Eng. **87**(9), 1792 (2010). https://doi.org/10.1016/j.mee.2009.10.016
18. K. Kano, K. Arakawa, Y. Takeuchi, M. Akiyama, N. Ueno, N. Kawahara, Sens. Actuators A **130–131**, 397 (2006). https://doi.org/10.1016/j.sna.2005.12.047
19. A.T. Tran, O. Wunnicke, G. Pandraud, M.D. Nguyen, H. Schellevis, P.M. Sarro, Sens. Actuators A **202**, 118 (2013). https://doi.org/10.1016/j.sna.2013.01.047
20. C. Zuo, N. Sinha, G. Piazza, Sens. Actuators A **160**(1–2), 132 (2010). https://doi.org/10.1016/j.sna.2010.04.011
21. E. Herth, F. Lardet-Vieudrin, L. Valbin, E. Algré, in Proceedings of the 2015 Symposium on Design, Test. Integration and Packaging of MEMS/MOEMS (DTIP), vol. 2015 (2015), pp. 1–5. https://doi.org/10.1109/DTIP.2015.7160996
22. A. Andrei, K. Krupa, M. Jozwik, P. Delobelle, L. Hirsinger, C. Gorecki, L. Nieradko, C. Meunier, Sens. Actuators A **141**(2), 565 (2008). https://doi.org/10.1016/j.sna.2007.10.041
23. N. Sinha, G.E. Wabiszewski, R. Mahameed, V.V. Felmetsger, S.M. Tanner, R.W. Carpick, G. Piazza, Appl. Phys. Lett. **95**(5), 053106 (2009). http://ieeexplore.ieee.org/xpls/abs_all.jsp?arnumber=5198318
24. R. Lanz, P. Muralt, IEEE Trans. Ultrason. Ferroelectr. Freq. Control **52**(6), 938 (2005)
25. A. Samarao, F. Ayazi, in Proceedings of the 2011 IEEE 24th International Conference on Micro Electro Mechanical Systems (MEMS) (2011), pp. 169–172. https://doi.org/10.1109/MEMSYS.2011.5734388
26. D.T. Phan, G.S. Chung, Appl. Surf. Sci. **257**(20), 8696 (2011). https://doi.org/10.1016/j.apsusc.2011.05.050
27. R. Yoshizawa, H. Miyake, K. Hiramatsu, Jpn. J. Appl. Phys. **57**(1S), 01AD05 (2017). https://doi.org/10.7567/jjap.57.01ad05
28. M.X. Wang, F.J. Xu, N. Xie, Y.H. Sun, B.Y. Liu, Z.X. Qin, X.Q. Wang, B. Shen, CrystEngComm **20**(41), 6613 (2018). https://doi.org/10.1039/C8CE00967H
29. U. Schmid, H. Seidel, J. Vac. Sci. Technol. A **24**(6), 2139 (2006). https://doi.org/10.1116/1.2359739
30. G. Guisbiers, L. Buchaillot, Nanotechnology **19**(43), 435701 (2008). https://doi.org/10.1088/0957-4484/19/43/435701
31. E. Herth, E. Algré, B. Legrand, L. Buchaillot, Microelectron. Eng. **88**(5), 724 (2011). https://doi.org/10.1016/j.mee.2010.06.032
32. J.O. Olowolafe, R.E. Jones, A.C. Campbell, R.I. Hegde, C.J. Mogab, R.B. Gregory, J. Appl. Phys. **73**(4), 1764 (1993). https://doi.org/10.1063/1.353212
33. I. Horcas, R. Fernández, J.M. Gómez-Rodríguez, J. Colchero, J. Gómez-Herrero, A.M. Baro, Rev. Sci. Instrum. **78**(1), 013705 (2007). https://doi.org/10.1063/1.2432410
34. G. Guisbiers, O.V. Overschelde, M. Wautelet, P. Leclère, R. Lazzaroni, J. Phys. D: Appl. Phys. **40**(4), 1077 (2007). https://doi.org/10.1088/0022-3727/40/4/024
35. G. Guisbiers, L. Buchaillot, J. Phys. D: Appl. Phys. **41**(17), 172001 (2008). https://doi.org/10.1088/0022-3727/41/17/172001
36. G. Guisbiers, D. Liu, Q. Jiang, L. Buchaillot, Phys. Chem. Chem. Phys. **12**(26), 7203 (2010). https://doi.org/10.1039/C002496A
37. N. Naumenko, P. Nicolay, Appl. Phys. Lett. **111**(7), 073507 (2017). https://doi.org/10.1063/1.4985582
38. T. Aubert, O. Elmazria, B. Assouar, L. Bouvot, M. Oudich, Appl. Phys. Lett. **96**(20), 203503 (2010). https://doi.org/10.1063/1.3430042
39. L. Vergara, J. Olivares, E. Iborra, M. Clement, A. Sanz-Hervás, J. Sangrador, Thin Solid Films **515**(4), 1814 (2006). https://doi.org/10.1016/j.tsf.2006.07.002
40. H. Miyake, C.H. Lin, K. Tokoro, K. Hiramatsu, J. Cryst. Growth **456**, 155 (2016). https://doi.org/10.1016/j.jcrysgro.2016.08.028
41. B. Liu, J. Gao, K. Wu, C. Liu, Solid State Commun. **149**(17–18), 715 (2009)
42. F. Medjani, R. Sanjines, G. Allidi, A. Karimi, Thin Solid Films **515**(1), 260 (2006)
43. S. Priya, H.-C. Song, Y. Zhou, R. Varghese, A. Chopra, S.-G. Kim, I. Kanno, L. Wu, D.S. Ha, J. Ryu, RG. Polcawich, Energy Harvest. Syst. **4**(1), 3 (2017). https://doi.org/10.1515/ehs-2016-0028. https://www.degruyter.com/view/j/ehs.2017.4.issue-1/ehs-2016-0028/ehs-2016-0028.xml

Publisher's Note Springer Nature remains neutral with regard to jurisdictional claims in published maps and institutional affiliations.